analytical chemistry

pubs.acs.org/ac Article

Digital Processing for Single Nanoparticle Electrochemical Transient Measurements

Salvador Gutierrez-Portocarrero, Kiley Sauer, Nelum Karunathilake, Pradeep Subedi, and Mario A. Alpuche-Aviles*

Cite This: *Anal. Chem.* 2020, 92, 8704–8714 Read Online

ACCESS | Metrics & More | Article Recommendations | Supporting Information

ABSTRACT: We demonstrate the use of digital frequency analysis in single nanoparticle electrochemical detection. The method uses fast Fourier transforms (FFT) of single entity electrochemical transients and digital filters. These filters effectively remove noise with the Butterworth filter preserving the amplitude of the fundamental processes in comparison with the rectangle filter. Filtering was done in three different types of experiments: single nanoparticle electrocatalytic amplification, photocatalytic amplification, and nanoimpacts of single entities. In the individual nanoparticle stepwise transients, low-pass filters maintain the step height. Furthermore, a Butterworth band-stop filter preserves the peak height in blip transients if the band-stop cutoff frequencies are compatible with the nanoparticle/electrode transient interactions. In hydrazine oxidation by single Au nanoparticles, digital filtering does not complicate the analysis of the step signal because the stepwise change of the particle-by-particle current is preserved with the rectangle, Bessel and Butterworth low pass filters, with the later minimizing time shifts. In the photocurrent single entity transients, we demonstrate resolving a step smaller than the noise. In photoelectrochemical setups, the background processes are stochastic and appear at distinct frequencies that do not necessarily correlate with the detection frequency (f_p), of TiO_2 nanoparticles. This lack of correlation indicates that background signals have their characteristic frequencies and that it is advantageous to perform filtering a posteriori. We also discuss selecting the filtering frequencies based on sampling rates and f_p. In experiments electrolyzing ZnO, that model nanoimpacts, a band-stop filter can remove environmental noise within the sampling spectral region while preserving relevant information on the current transient. We discuss the limits of Bessel and Butterworth filters for resolving consecutive transients.

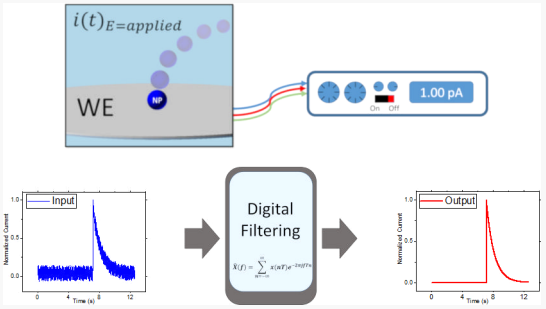

Studies on electrochemical processes on individual NPs aim to understand the particle-by-particle contribution to an ensemble process, for example, in an electrocatalytic cell where NP ensembles carry out a catalytic reaction or to improve the limits of detection in analytical applications that use nanostructures as tags.[1] Single NP studies yield insights into NPs reactivity and its statistical distribution in electrocatalysis, colloidal reactions, catalysis, and photocatalysis.[2−13] NP electrochemical studies are described as stochastic electrochemistry,[3,8,14] nanoimpact,[5,15−17] experiments that trap a single NP on an electrode surface.[18−21] Additionally, reports of scanning electrochemical microscopy (SECM),[22] and scanning electrochemical cell microscopy (SECCM)[23] address individual NPs on a substrate. These experiments share the challenge of requiring small current measurements, typically in the order of pico-amps, and therefore, it is essential to design a strategy to discriminate against noise to achieve single NP detection. Noise discrimination is necessary for analytical applications where the NPs are tags for specific analytes, and to obtain reliable mechanistic information from the experimental data. In nanoimpact experiments, the NP is electrolyzed when it collides with the electrode surface, e.g., Ag (NP) → Ag^+. Therefore, the current is limited by the NP size and the total charge required to electrolyze the NPs. In analytical applications, the Ag NPs serve as tags for analyte detection, where the NPs collide at a disk electrode surface at their diffusion-limited rate, with a diffusional collision frequency, $f_{p,d}$[4,8]

$$f_{p,d} = 4D_{NP}r_d C_{NP}^{bulk} \quad (1)$$

where D_{NP} is the diffusion coefficient of the NP, r_d is the radius of the disk electrode, and C_{NP}^{bulk} is the average NP bulk concentration. As NP diameter decreases D_{NP} increases its value, and according to eq 1, this leads to a higher $f_{p,d}$; in turn, the higher number of nanoimpacts makes the NP easier to

Received: November 18, 2019
Accepted: June 8, 2020
Published: June 8, 2020

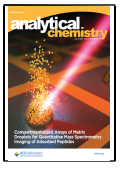

https://dx.doi.org/10.1021/acs.analchem.9b05238
Anal. Chem. 2020, 92, 8704–8714

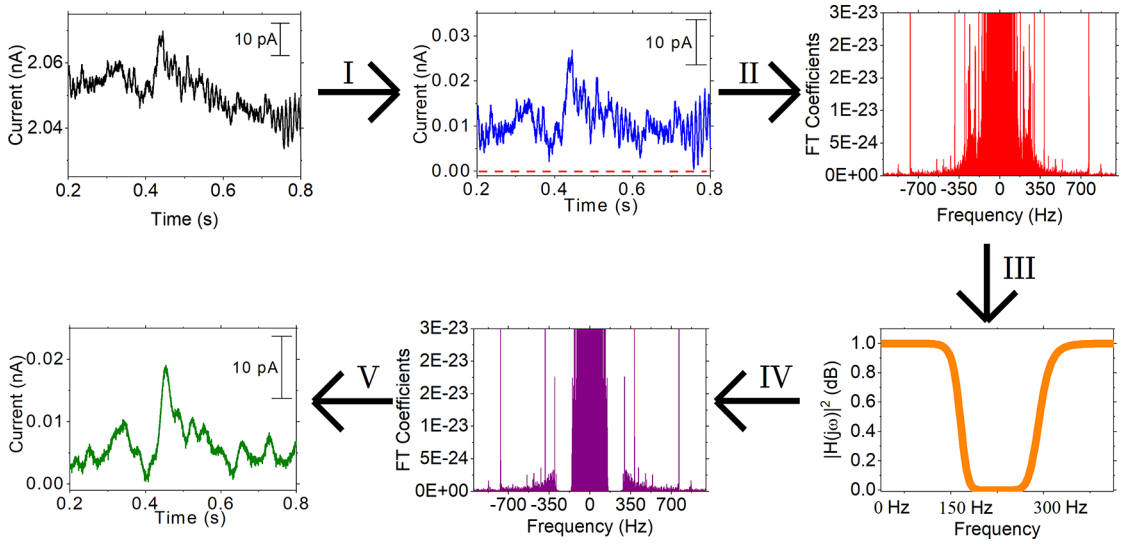

Figure 1. Schematic representation of the filtering procedure: (I) removing an offset, if necessary. (II) FFT to generate the frequency spectrum, up to this point, the procedure is repeated with the blank signal input to design the filter, (III) filter design (transfer function), (IV) multiplication of functions in the frequency domain, and (V) inverse FFT to generate the time-dependent output signal and, if necessary, restore the original offset.

detect. However, smaller NPs will intrinsically have a lower detection charge, because there are fewer atoms to electrolyze. A similar challenge exists in electrocatalytic amplification, where NPs active toward a reaction collide with an inert electrode. For example, hydrazine oxidation reaction 2 serves as a detection mechanism for NPs interacting with the working electrode:[8,24]

$$N_2H_4 \rightarrow N_2 + 4H^+ + 4e \quad (2)$$

Here again, the diffusion rate and the frequency of collision will be larger for smaller NPs, eq 1, but the current is limited by the active surface area of the NP, and the smaller NPs will require a more robust signal-to-noise (S/N) discrimination. In mechanistic studies, it would be of interest to study smaller NPs and possible quantum confinement effects. However, these studies will require smaller NPs and, in turn, methods to discriminate against noise because they will likely be performed near the limits of available instrumentation.

In this paper, we present a digital filtering approach to discriminate against noise in three challenging single entity applications. Digital filtering and smoothing are widely used in spectroscopy,[25,26] in nuclear magnetic resonance (NMR)[27,28] and in Fourier-transformed infrared spectroscopy (FTIR).[29] However, its use in electrochemistry is less common than analog filtering. De Levie used digital smoothing on the numerical differentiation of electrochemical interfacial tension data.[30] The application of fast Fourier transform (FFT) to polarography was reported,[31] and Smith et al. proposed digital smoothing to improve peak potential detection. Their method discriminates against low-frequency noise or "drift" and yields more accurate peak currents in cyclic voltammetry (CV).[32,33] Wipf et al. used digital filtering to improve the S/N ratio on fast-scan cyclic voltammetry (FSCV) with a trapezoidal filter.[34] Since then, Heien points out that Butterworth filters have been used to analyze FSCV data acquired with different potential waveforms.[35−37] More recently, Heien et al. used advanced filtering to improve dopamine detection with a two-pass infinite impulse response filter (a "zero phase shift" filter).[35] Little et al. used digital filtering during nanoimpacts to aid in data analysis.[38] Instrumentation effects have been described before using digital methods,[38−41] as discussed below, but we propose that digital processing can be used as the main filtering strategy, and we discuss its limitations.

Our results demonstrate the use of digital filters to enhance the S/N in single entity experiments effectively. We use FFT methods to transform the time-dependent electrochemical data into the frequency domain, analyze it, and filter detrimental frequency components. Therefore, we present an effective discrimination strategy utilizing the frequency domain to determine systematically what regions of the frequency domain correspond to the signal of interest to discriminate it from random and electronic noise. We show that the selective removal of a frequency domain can reduce the noise while preserving the relevant information on the transients due to single element interactions with an electrode, down to an individual NP. We focus on two filters, the "rectangle filter" (an extreme case) and the Butterworth filter, on three single entity processes. We compare these two filters with low-pass Bessel filters and Hamming windowing functions. We note that the rectangle filter is also called a "boxcar brick wall" filter. Thus, we use the rectangle filter to avoid confusion with the widely used boxcar integration in analytical applications. We performed this digital filtering with widely available software and computing hardware, and we discuss how the use of these digitizing techniques can aid in the design of customized instrumentation for single NP studies.

THEORY

The analysis of the experimental current vs time data is done in the frequency domain by FFT. Moreover, the frequency spectrum is obtained with the discrete-time Fourier transform (DTFT) method using commercial software (Matlab). Here, we briefly describe the critical aspects of the DTFT method with more details in the Supporting Information (SI, section 1) taken from the relevant literature.[42−45] The spectrum of the sampled signal, $\hat{x}(t)$, is represented by $\hat{X}(f)$:[42−44]

$$\hat{X}(f) = \sum_{n=-\infty}^{\infty} x(nT)e^{-2\pi jfTn} \quad (3)$$

https://dx.doi.org/10.1021/acs.analchem.9b05238
Anal. Chem. 2020, 92, 8704−8714

Table 1. Diffusional Properties, Sampled Frequencies, and Analog Filtering Conditions Used in This Work

conditions	NP radius[a] (nm)	D_{NP} (cm^2/s) × 10^{-8}	C_{NP}^{bulk} (pM)	f_p (Hz)	f_s (Hz)	analog filtering
Figure 2, 10 mM, hydrazine, 50 mM PBS, pH 7.4	19 ± 2	14 ± 10	30	3	122	none
Figure 3 and 4, CH_3OH	144 ± 52	2.75 ± 0.04	0.05	0.002	50	150 kHz
Figure 5, CH_3CN	7(8 ± 1)[b]	3.8 ± 0.4	70	3	6250	150 kHz

[a]Average NP diameter by TEM. [b]Mostly agglomerates present in suspension Figure 6a,b.

where the continuous input signal, $\hat{x}(t)$, is converted to a discrete sequence of sampled values and expressed as the so-called discrete-time signal, $x(nT)$. The total experimental time is $t = nT$, where T is the sample interval and nT is the time for the nth sample, $j = \sqrt{-1}$ and all of the other symbols have their usual meaning. The sampling frequency in Hz is $f_s = 1/T$. The Nyquist interval, eq 4, is a characteristic of the DTFT method that restricts the sample frequencies to[45]

$$-\frac{f_s}{2} < f < \frac{f_s}{2} \tag{4}$$

The Fourier spectrum, within limits imposed by the Nyquist interval, allows one to analyze the power distribution of noise on the frequency range. Based on the analysis, one selects the frequency range to filter using a transfer function that describes the digital filter and transforms the original function into the smoothed final output. In practice, these operations are done with a normalized frequency, ω (see the SI for details), and to obtain the smooth function, $Y(\omega)$, one multiplies the discrete sampled function, $X(\omega)$, and the filtering transfer function, $H(\omega)$:[45]

$$Y(\omega) = H(\omega)X(\omega) \tag{5}$$

Figure 1 shows the schematics of the filtering process that involves the following steps: (I), if necessary, remove any obvious DC offset to minimize problems with DTFT, in this paper, we subtract the minimum y value to the full data set, to make the minimum pass through $y = 0$. (II) Transform the time-domain discrete function into the frequency domain by DTFT. (III) Identify the frequency or range of frequencies to remove and design the appropriate filter. (IV) Multiply the filtering function, $H(\omega)$, with the signal input in the frequency domain, and (V) calculate the inverse DTFT[32,33,46] and restore any offset removed in step (I). Transfer functions are symmetric in the Nyquist interval of the FFT spectrum, although it is customary to represent them in just the positive frequency domain.

Rectangle Low-Pass Filter. The simplest filter that we can use is the so-called rectangle filter, characterized by a sharp cutoff at the ω_c shown in Figure S1. Moreover, under the conditions of this work, this is the easiest way to filter and obtain satisfactory results, e. g., it yields the smallest time delay. On the other hand, it generates more evident ringing in the signal and overshoot (e.g., Figure S4).

Butterworth Band-Stop Filter. Like in the filtering procedure for rectangle filtering, we design a Butterworth filter after selecting the frequency range to be attenuated. For every experiment, the frequency range to be mitigated was selected based on the background and the fundamental frequency intrinsic to the measurement, as discussed below (e.g., Table 1). For a low pass Butterworth filter, the transfer function is

$$|H(j\omega)|^2 = \frac{1}{1 + \left(\frac{j\omega}{j\omega_c}\right)^{2n_f}} \tag{6}$$

where n_f is the filter order and ω_c the so-called cutoff filtering in radians. In this work, $n_f = 3$ and 3-dB the attenuation at the cutoff frequency. The band-stop Butterworth filter is characterized by a series of parameters that are defined as a function of the frequencies ω_{pa} and ω_{pb}, so that the band to filter is $\omega_{pa} \leq \omega \leq \omega_{pb}$, as shown in eq 7.[44,45] Finally, signal outputs are generated using eqs 6 and 7 as the filtering functions. The outputs are compared to the rectangle function (see the SI, section 3).

$$H_i(z) = \frac{G_i(1 - 2cz^{-1} + z^{-2})^2}{1 + a_{i1}z^{-1} + a_{i2}z^{-2} + a_{i3}z^{-3} + a_{i4}z^{-4}} \tag{7}$$

To design a band-stop filter the algorithm is derived from a bilinear transformation method (see the SI, section 3).[45] Briefly, the band-stop filter is designed with two normalized frequencies, $0 \leq \omega \leq \omega_{pa}$ and $\omega_{pb} \leq \omega \leq 1$, to yield the combined band stop $\omega_{pa} \leq \omega \leq \omega_{pa}$, see Figure S2.

EXPERIMENTAL SECTION

Current vs time (i–t) transient experiments were performed using a three-electrode cell and a commercial potentiostat, CHI 760 (CH Instruments, Austin, TX). All experiments were performed inside a Faraday cage. A platinum wire electrode was used as a counter electrode (CE). The working electrode (WE) was an ultramicroelectrode (UME) fabricated as described before.[47,48] Different electrodes were prepared with diameters around 10 μm, unless otherwise stated. Materials were characterized by powder X-ray diffraction and transmission electron microscopy (TEM, JEOL 2100F). NP suspensions were characterized by dynamic light scattering (DLS) using a commercial system Particle Sizing 380 ZLS (Particle Sizing Systems NICOMP, Santa Barbara, CA).

Au NP Collisions. We followed the previously reported experimental conditions.[3,8,14,49] Briefly, the reference electrode (RE) was Ag/AgCl (KCl = 1 M), and the WE was a 6 μm diameter carbon fiber UME. Collision studies were done in 10 mL of 10 mM hydrazine, 50 mM PBS solution at a pH of 7.4. The solution was bubbled with Ar gas for 20 min and was kept under an Ar blanket. A 5 μL aliquot of Au NPs was then added to the solution. Current transient experiments (i–t) were run at an applied potential of 0.47 V vs Ag/AgCl. In a typical experiment, the sample interval used was 0.00819 s (f_s = 122 Hz) and the sensitivity was set to 1×10^{-9} A/V. The NPs were characterized by TEM and DLS (Figure 2a,b, more details below).

TiO_2 NP Collisions. Photoelectrochemical experiments were performed following a procedure modified from prior reports.[9,50,51] A platinum wire electrode was used as a CE. The RE was a homemade electrode previously reported[52] with the final cell arrangement Pt/I^-,I_3^-, TBAP, MeOH/Pt/MeOH//.

https://dx.doi.org/10.1021/acs.analchem.9b05238
Anal. Chem. 2020, 92, 8704–8714

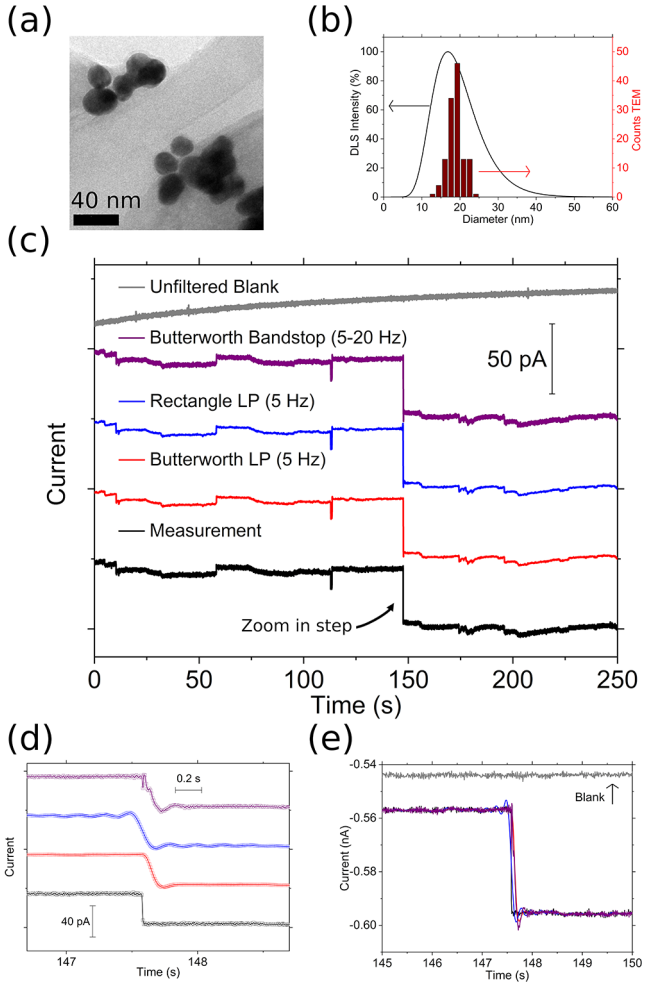

Figure 2. (a) Current transient for single Au NPs with at 6 μm diameter C-fiber UME. (b) NP size distribution by TEM (bars) and by DLS (curve) (c) Current vs time traces after filtering with different types of digital filters, compared with the unfiltered data (labeled "measurement") and blank. The arrow shows the step studied in detail. (d) Detail of a single NP transient showing filtering effects. There is an offset in the y direction for clarity in (d), and the data without offset is shown in panel e. Filter description: Butterworth LP is a low-pass filter (5 Hz cutoff filters); all Butterworth filters are third order. NP suspension: 3 pM Au NPs, 50 mM PBS buffer pH 7.4 and 10 mM hydrazine. E_{app} = 0.475 V vs Ag/AgCl.

The WE was a platinum disk UME. Initially, 9.5 mL of spectrophotometric grade methanol (≥99.9%, Fisher) were deoxygenated with N_2 for 30 min, and an aliquot of NP suspension is added during the experiment. The applied potential was E_{app} = 0.0 V vs I^-/I_3^- (20 mM TBAI) = 0.38 V vs NHE; these experimental conditions have been reported elsewhere,[9] but in this paper we use a continuous wave laser of HeCd (λ = 325 nm, IK3501R-G, Kimmon Koha U.S.A., Inc.) as photon source (Figures 3 and 4). Here, a 500 μL aliquot of suspension of TiO_2 NPs was added to the methanol solution, after 60 s of running the $i-t$ transient experiment to collect a background signal. The concentration of the colloidal suspension of TiO_2 NPs stock solution was 50 fM. The sample interval used was 0.02048 s (f_s = 50 Hz). Finally, the sensitivity was set to 1 × 10^{-9} A/V. The TEM mean diameter of the NP is [144 ± 52] nm (Figure 3a,b) and the crystalline phase of the particles is anatase as shown in the XRD Spectrum (see Figure S9 in the SI for details). Fourier spectra of

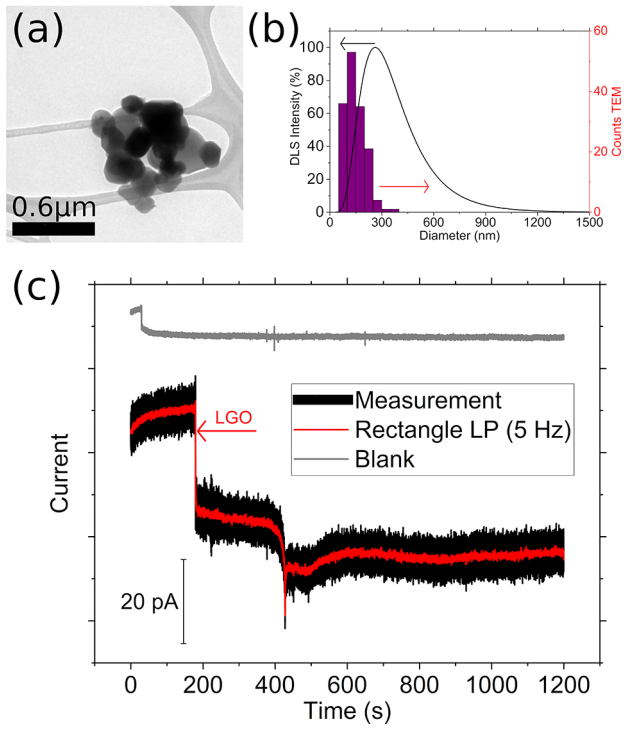

Figure 3. (a) TEM of TiO_2 NPs agglomerated. (b) TEM (bars) and DLS (curve) size distribution for a suspension and (c) current transients for TiO_2 NPs suspension with at 10 μm diameter Pt UME. LGO marks the opening of the laser gate at 180 s for the TiO_2 experiment. In the blank LGO at 30 s. At a previous experiment, NPs were spiked into the MeOH suspension for a final concentration of 50 fM.

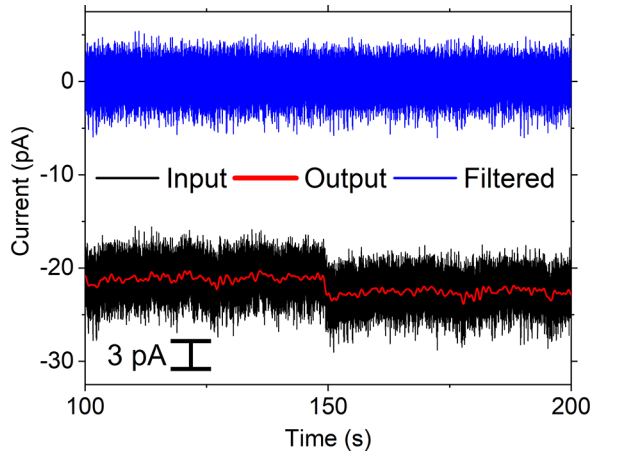

Figure 4. Current transients for TiO_2 NPs of 18 nm diameter on Pt UME of 10 μm diameter. The data was filtered with a rectangle filter, f_c = 5 Hz. All other conditions as in Figure 3.

chronoamperograms for the blank, i.e., before collisions, and during collisions are shown in Figure 5.

ZnO NP Collisions. The conditions have been reported elsewhere;[41,53] briefly, the RE was an aqueous Ag/AgCl (KCl = 1M). The CE and the RE were separated with fritted glass filled with acetonitrile to avoid cross-contaminating with the WE compartment. The WE was a mercury hemisphere UME prepared by a procedure reported previously.[53,54] Briefly, 9.5 mL of HPLC grade acetonitrile was bubbled with Ar for 30 min. Current transients were run at an applied potential of

https://dx.doi.org/10.1021/acs.analchem.9b05238
Anal. Chem. 2020, 92, 8704−8714

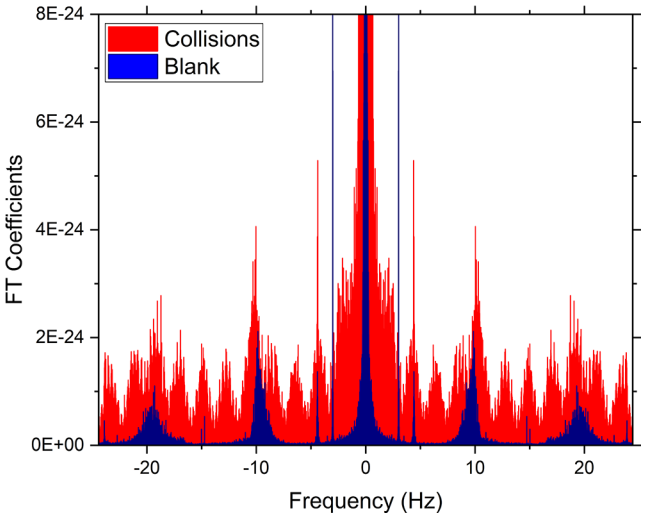

Figure 5. Fourier spectrum of methanol (blue) and suspension after the NP suspension spike without filtering (red, all other conditions as in Figure 3).

−2.4 V vs Ag/AgCl. A 500 μL aliquot was spiked to the solution so that the final concentration ZnO NPs in the cell was 10 nM. The concentration of 52 nm diameter ZnO agglomerates (by DLS and TEM Figure 6a,b) is 70 pM. The sample interval was 0.0002 s, and the sensitivity was set to 1×10^{-9} A/V. The TEM mean diameter of the NP is [8 ± 1] nm,

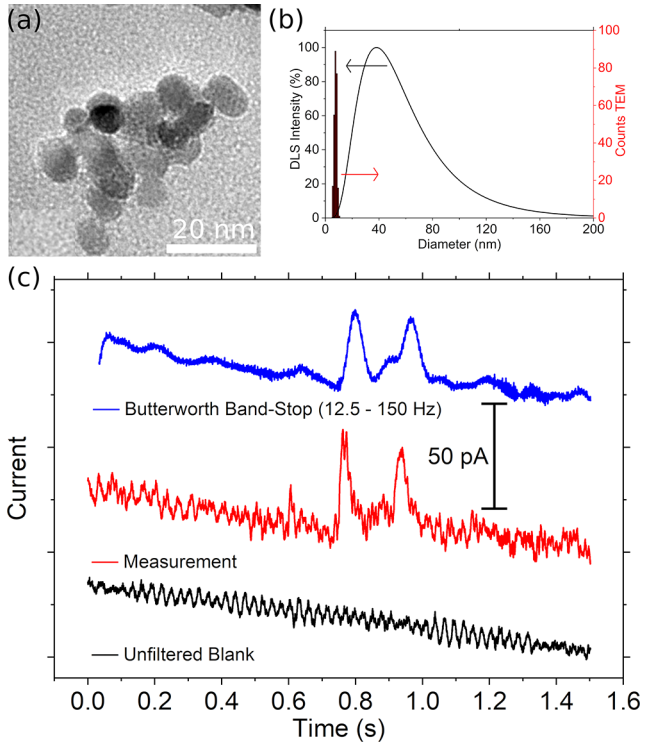

Figure 6. (a) ZnO NPs used in a suspension for stochastic measurements of the reduction of ZnO to Zn(Hg). (b) Size distribution measured by TEM (bars) and DLS data (curve). (c) Current transients after a BW band-stop filter (blue) without filtering (measurement, red) compared with the unfiltered blank. ZnO NPs collisions on 12.5 μm diameter Hg UME in a 10 nM ZnO NP concentration in CH_3CN.

and the crystalline phase of the particles is zincite, according to the XRD (see Figure S8 in the SI for details).

RESULTS AND DISCUSSION

Au NP Collisions. We analyzed a system where the S/N ratio is high to check the filtering effect on time shift and signal distortion on single NP measurements. Figure 2 shows the collisions of Au NPs enhanced by the electrocatalytic reaction of hydrazine oxidation, reaction 2. This is a highly reproducible system that can be compared with other sizing techniques since agglomeration is not as problematic as with other systems (TiO_2 and ZnO).[9,53] Further, the parasitic capacitance from the NP-electrode interface, connectors, Faraday cage, and instrumentation issues are minimized.[55] Therefore, we obtained a relatively large collision current transient (40 pA), with negligible noise contributions (cf. baseline Figure 2C), and we tested the effect of filtering on the shape of the $i-t$ response.

Figure 2b shows the NP size distribution by TEM (bars) and by DLS (curve), which is consistent with dispersed NPs given the overlap of the two distributions. Further, the size of individual transients is consistent with individual NPs interacting with the carbon WE. As discussed in the SI, section 4, the current observed in these experiments is due to singe NP oxidizing hydrazine at the diffusion-limited rate (observed 40 pA vs the 44 pA expected from theory).[8,24,56,57]

The diffusion-limited oxidation current for a particle supported on a partially blocking substrate, $i_{d,l}$, is given by

$$i_{d,l} = 4\pi \ln(2) nDC^* r_{NP} \quad (8)$$

where n is the number of electrons, F is Faraday's constant, D and C^* are the diffusion coefficient and the bulk concentration of hydrazine, and r_{NP} is the radius of the particle.[8] The transients in Figure 2c that correspond to the data as it was collected, i.e., before filtering on the trace labeled as "measurement", are due to single NPs colliding with the inactive C surface (e.g., at 147 s, $i \approx 40$ pA, indicating a single NP event).[8] Figure 2c shows the filtering effect with both algorithms for low pass (LP) filters with a cutoff frequency of 5 Hz. For the LP rectangle filter (blue), the shape of the current step is preserved, but the output signal show ripples in the transient; this is a well-known problem of using a rectangle LP filter and corresponds to an extreme case. On the other hand, the Butterworth filter output shows fewer problems with signal distortion while it does introduce a small delay in the time domain, discussed below, for the LP and band-stop (purple and red in Figure 2d). Note, however, that all of the digital filters preserve the step current size for the single NP transient (Figure 2e). Also, for the LP Butterworth filter, we observe an overshoot (expected).[58] We tested the effect of the digital filters on a step function and determined the figures of merit of the different filters: Bessel, Butterworth, and rectangle along with the Hamming windowing function used in FFT filtering. We use previously defined values of merit,[59] and we include a time shift for the signal to reach 50% (t_{50}) to quantify the filter delay (SI, section 5, Figure S3). The step had the same time interval as the experimental data in Figure 2, and we present the filters' response in Figure S4, with the figures of merit compiled in Table S2. The Bessel and Butterworth filters provide similar responses as expected.[59] The Bessel function has a lower overshoot (0.75%) with respect to the Butterworth (8.3%), while the Butterworth response has shorter rise time

https://dx.doi.org/10.1021/acs.analchem.9b05238
Anal. Chem. 2020, 92, 8704−8714

and delay, t_{50}. The largest overshoot is for the rectangle (8.8%), so in applications where the noise is larger than 10% of the transient, a simple rectangle filter is an effective tool to guide the design of more complex filters. The filtering of the experimental step at 20 s in Figure 2 shows similar responses given in Table S3, with the experimental noise resulting in slower time responses (rise time, t_r and $t_{50\%}$) compared to the theoretical step. Note that the Hamming windowing function, although having a faster response, does not provide effectively filtering at low orders (5th order) and requires high orders to have significant attenuation (100th); these higher-order functions come at the expense of slower response times. We prefer the faster Butterworth filter because of analytical applications that measure time to determine concentration.[60] The time it takes to observe the first collision or time of first arrival (TFA) measures NP concentration. For the migration-limited case, NP concentration is proportional to 1/TFA,[60] and a delay in the data due to filtering will introduce an error in concentration (see below). For a 1 fM concentration, a TFA of 100 s has been reported,[60] and if digital filtering resulted in a delay of $t_{50\%}$ = 0.2 s, this will introduce an error of −0.2%. The filters used here have $t_{50\%}$ < 200 ms and will introduce an error smaller than 0.2%, except for the Hamming 100th order. The time delay for the Butterworth is the result of the slowest term in the digital filter series.[61]

$$t_{50\%} \approx \frac{k_{del}}{f_c} \tag{9}$$

where k_{del} depends on the filter order. For the third order filter used in this work[61] $t_{50\%} \approx 0.318/f_c$ (f_c in Hz) which is a good approximation for the values listed in the SI tables for the low pass filter: Tables S2 and S3 for simulated and experimental steps, respectively. For the band stop filters, which are linear combinations of a low pass and a high pass filter, the slowest term determines the delay, so eq 9 applies when f_c is the lower frequency of the band-stop limit, cf. Table S4 (delays for data in Figures 2 and 6).

In the SI, Figure S5 shows a current spike due to agglomeration on an edged solution where the current is larger (up to 100 pA, Figure S5A), and thus, the S/N is significant, and we can test for signal distortion due to filtering. Again, the output signal shows ripples in the transients using a rectangle low pass filter. In contrast, the Butterworth filter output shows fewer distortions, and while it does introduce a small delay in the time domain, the shape of the transient is preserved (Figure S5B). Preserving the shape is of interest because the shape of the transient carries information about the dynamics of the collision process.[62−65] A low pass Butterworth zero-phase shift filter has been reported for FSCV,[35,66] but because we use a band-stop filter, we have not attempted to compensate for the phase shift of the signal. Instead, we have chosen the filtered frequency components in a way that minimizes the shift. However, the change is not important if the steady-state current or step size is the critical parameter, such as in detection applications that use the steady-state current, e.g., eq 8

Photocatalytic Collisions. The experiments where the semiconducting NPs are under constant illumination, as described in the Experimental Section, present additional challenges when improving the S/N ratio. For example, a Faraday's cage must allow light into the cell, which in turn reduces the shielding effectiveness. Also, the setup can introduce additional noise, e.g., the laser's power supply. Here we demonstrate the use of digital filtering on the $i-t$ trace. Figure 3 shows the photocurrent transients for 144 ± 52 nm TiO_2 NPs (TEM, Figure 3a). The NP size distribution by TEM (bars, Figure 3b) and DLS (curve, Figure 3b) of the NPs used to give the current trace in Figure 3c at E_{app} = 0.0 V vs I^-/I_3^- (20 mM TBAI). The experiment starts in the dark (no illumination), and later, the laser gate is opened (LGO), and we injected a colloidal suspension of NPs into the cell to give a final concentration of 50 fM. The current transient here is 12 pA. Note that the DLS size distribution shifts toward higher diameters from the TEM size distribution, and therefore, the formation of agglomerates could be significant (Figure 3b). Also, aggregates can be observed from the TEM image (Figure 3a). As discussed above, the use of a rectangle LP filter preserves the signal transient, and the ripples introduced are not significant when compared to the noise present in the signal (see the blank experiment in Figure 3c). When the photocurrents are much smaller than those predicted by eq 8, this indicates that the process is under kinetic control. Therefore, S/N discrimination strategies are necessary to study the kinetics of electron transfer process under illumination. The expected overshoot for a rectangle filter is ca. 8%, but in the experimental conditions of Figure 3c, the noise is much larger, ca. 13 pA, complicating data analysis. Figure 4 shows the result of filtering a current transient with a 2.2 pA step. This current transient is not evident in the unprocessed data, but it is apparent after digital filtering. The noise (blue input trace obtained by subtracting the filtered signal from the unprocessed data) has an amplitude of ca. 10 pA, larger than the signal filtered. The use of the digital low-pass filter with f_c = 5 Hz, allows detection of a step with a smaller magnitude than the noise. Interestingly, it is possible to implement a rectangle filter with a simple code or a spreadsheet program.

Figure 5 shows the Fourier spectrum of the current transients in Figure 3 for a TiO_2 NP suspension in methanol. The spectrum showed an increase in the value of the Fourier coefficients for the collision (red traces) in comparison with the blank solution (blue). The Fourier coefficients increased because the addition of TiO_2 NPs to methanol, which indicates that the photocatalytic process introduces other stochastic phenomena. It is important to note that the blank was collected before the spiking of NPs with the same experimental conditions of illumination. Interestingly, adding TiO_2 NPs removes the 3 Hz component observed with the methanol/Pt(UME) interface (blank, blue in Figure 4). The Fourier spectrum of the TiO_2 collisions (red) does not show the peak at 3 Hz; in contrast, the noise around 10 and 20 Hz is evident in the background and TiO_2 agglomerate collisions. Therefore, these results indicate that the background processes have distinct frequencies that do not necessarily correlate with the NP collision data. After examining the FFT spectrum (red in Figure 4), we selected a low pass filter at 5 Hz. Note that the frequency cutoff is above the frequency of collisions, f_p = 0.002 Hz (Table 1).

We consider the relevant frequency domain for single entity measurements based on four factors. (a) The fundamental stochastic frequency defined by eq 1a (eq 1, restated)[4]

$$f_{p,d} = 4D_{NP}r_dC_{NP}^{bulk} \tag{1a}$$

https://dx.doi.org/10.1021/acs.analchem.9b05238
Anal. Chem. 2020, 92, 8704−8714

where D_{NP} is a function of the NP size distribution depending on factors such as agglomeration. Values of frequency of collisions, f_p, can vary widely because it is also a function of concentration, and of the working electrode size. Table 1 shows the expected values for the NPs used in this work, and by manipulating concentrations, the diffusional frequency, $f_{p,d}$, is in the order of 1 Hz, except for Figure 5, where we discuss higher frequency events. (b) The type of information sought: in analytical applications where a current step needs to be above the noise level, the step height is defined by eq 8 (Figure 2c−e) while the frequency of collision yields NP concentration (eq 1). Also, the shape of the transient contains information about NP/electrode interactions, which may require higher values of f_s. Therefore, a band-stop filter gives appropriate filtering without modifying the time-dependent signal significantly. (c) Instrumental limitations: in our current instrumentation, we estimate a rising time of approximately 12 ms with 150 kHz hardware filtering,[51] in line with other reports.[67] Therefore, in this work we have used higher hardware frequency cutoff or no filtering at all (Table 1). These factors explain why the sampling frequency for single NP experiments remains the object of investigation.[64,68] Robinson et al. simulated the filter behavior to design low-pass Bessel analog filters.[68] For example, events at higher frequencies than f_p are common in single entity experiments because NPs can bounce off the electrode surface to recollide multiple times.[63,65,69] Furthermore, for a single 33 nm Ag NP interacting with an electrode, 6 ns pulses are expected as the NP travels across the electrode surface.[64] To resolve these quick Brownian motion transients will require sampling in the MHz domain and currently available instrumentation cannot resolve these transients.[68] (d) From a data acquisition point, the Nyquist frequency to resolve transients requires at least two times the fundamental frequency to sample a sinusoidal wave. For stochastic events, if we take f_p as the fundamental process frequency, we get a lower boundary of $f_s \geq 5f_p$, following the usual practice of sampling at higher frequencies for arbitrarily shaped signals (up to 10 times the fundamental frequency).[70] However, the details of the electrode NP interaction require frequencies much higher than f_p to resolve the fast frequency components, e.g., kinetics.[51,67] Single entity events occur over a wide range of frequencies, so it is complicated to design low-pass filters widely used in other electroanalytical applications because a low pass filtering could remove high-frequency components of interest. In order to circumvent this problem, we use digital band-stop filtering. This protocol allows us to combine our highest available sampling rate while rejecting the noise at intermediate regions of the frequency domain.

ZnO NP Collisions. We chose the electrolysis of ZnO NPs on a Hg electrode as a test for the so-called nanoimpacts. Figure 5 shows a relatively high-resolution data for the electrolysis of ZnO NPs with a nominal diameter of 8 nm (Figure 5a). The size distribution of the NPs measured by TEM (bars) is shown in Figure 5b and compared with DLS data (curve). Note that there is a significant shift in the DLS size, indicating that the agglomerates are the predominant species in the suspension.

The collision data was collected with a relatively high frequency 6 kHz (sample interval of 0.16 ms), to resolve transients that correspond to a single agglomerate reducing at the interface of the Hg UME.[53] The magnitude of the reduction charge per NP is proportional to the number of Zn atoms within a ZnO NP, thus the density and volume of the ZnO crystalline structure ($C \propto r^3$).[71] However, the shape of the transient is interesting in studies of NP electrolysis,[62−65] for example in the study of ZnO reduction kinetics.[41]

We demonstrate digital filtering to remove a frequency band from the signal. Here, we do not attempt to discuss the electron transfer transient, with some details given elsewhere.[41] For example, the blank shows the noise at 30 Hz, also seen in Figure S6, the FFT spectra of the data as collected and of the CH_3CN blank. In the blank's frequency spectrum, we can see peaks at 120, 180, etc., assigned to harmonics of the 60 Hz AC power and the interesting subharmonic of the power line (30 Hz). In Figure 6, we filtered the blank until a relatively flat line was obtained for the blank (Figure S7) with a 12.5 to 150 Hz band-stop giving the optimal results: to remove the periodic noise contributions and preserve the majority of the frequency spectrum.

Figure 6 shows the results of the band-stop filter from 12.5 to 150 Hz, which removes the AC noise. We also studied the digital band-stop filter with a Gaussian peak with a similar full width at half-maximum as the data in Figure 5c (SI, section 10). The filter effect includes a shift of 20 ms for the simulated peak, while in the filtered data, the first peak has shifted from 0.8 s, by about 40 ms (Table S4), which is expected based on the phase shifts of the filter. The simulated Gaussian peak after filtering (Figure S10) still contains 99.9% of the area of the unfiltered peak, consistent with the expectation that filtering in nanoimpact conditions preserves the peak area.[68,72] However, integrating the first filtered peak in Figure 5c at 0.8 s yields 3.83 pC, which is 96% of the unfiltered peak. We assign these differences to the difficulties of resolving the peak and the noise contributions in the data. Although there are several studies of low-pass filtering under single element electrochemical transients,[68,72] we are not aware of other studies using a band-stop filter like the one in this work.

Implications for Multiple Transients. It is of interest to investigate the limits of resolving single events. For example, two events that occur within a short time can be resolved if the sampling frequency is high enough and if the digital filtering does not remove an essential region of the Fourier spectra to resolve the transients. We investigate two closely spaced transients of the same area or with significant differences in areas. First, the resolution and the selected filter time constant are related. For example, White and co-workers[64] found that, to resolve a 0.1 ms pulse accurately, the cutoff frequency of the filter should be ≥30 kHz. Kanokkanchana et al.[39] proposed that 5−10 times faster filtering than the peak width to determine the peak height accurately. In general, the sampling rate needs to be faster than the frequency of the observed event, and Little et al.[38] used the Poisson equation to determine a minimum sampling rate for an experimental acquisition time, Δt_{exp}, which is chosen based on the fundamental frequency of single entity collisions on the electrode. The sampling frequency and the experimental transient time will be related by

$$f_s \geq k_{samp}(1/\Delta t_{exp}) \tag{10}$$

where k_{samp} is a constant that gives a higher sampling frequency to resolve the transient, e.g., $k_{samp} = 3$.

Second, we assume independent collisions at the specified sampling interval. Little et al.[38] discussed the sampling interval when measuring consecutive events, assuming that the events are independent from previous occurrences, the Poisson

https://dx.doi.org/10.1021/acs.analchem.9b05238
Anal. Chem. 2020, 92, 8704−8714

distribution describes the probability of nanoimpacts if they are genuinely stochastic (as discussed in detail in the SI, section 11). Here, we generalize the approach by considering that we need to measure over an interval Δt_{exp} where zero or one event will happen. Given that the single entity events have a mean rate, λ, the experimental time can be set to a certain probability of success of detecting one or zero events with a probability P_x. Therefore, collisions will occur at an average rate λ that is also the product between the time interval in eq 9 and the frequency of collisions, f_p.

$$\lambda = \Delta t_{exp} f_p \tag{11}$$

Combining eqs 10 and 11, we propose eq 12 that relates the frequency of collisions and the cutoff frequency with P_x = 99% of probability of zero or one event in the fixed time interval and with k_{samp} = 3 (see section S11 for details).

$$f_p \left[3\left(\frac{1}{f_s}\right)\right] \leq 0.141 \tag{12}$$

Equations 10−12 give the relationship between the required sampling interval to describe a single collision accurately (eq 10), given the frequency of collisions and sampling rate (eq 12). Note that without aggregation and assuming diffusion-limited conditions, $f_p \approx f_{p,d}$, given by eq 1. These equations agree with Compton and co-workers[38] that found vanishing peaks, i.e., features that were apparent only after they applied digital filtering[38] for a higher frequency than the one obtained with eq 11. They suggest a two-step protocol: (1) an analog filter chosen to resolve most transients followed by (2) a digital filter to remove noise further. Here, we use eqs 10−12 to provide minimum sampling frequencies to resolve the transients, and we propose that digital filtering can remove a posteriori the noise components. The higher limit for resolving transients is the potentiostat rise time that gives rise to a low-pass filter behavior. The instrument itself will provide the ultimate cutoff frequency with a potentiostat time constant of 3 ms, gives a higher sampling rate of $f_{c,inst}$ = 330 Hz, and according to eq 12, $f_p \leq$ 16 Hz, which is in line with our single NP detections here. For the higher f_s data here, we resolve transients of agglomerates where $f_p < f_{p,d}$; again, there is a difference between the diffusion-limited frequency and the actual frequency of collisions. Because eq 12 gives the expected results for 99% success probability of detecting one or zero collisions, we resorted to repetitive data collection to obtain a few collisions. The sampling rate was sufficient to resolve the transient because it was slowed by the electron transfer kinetics.[41]

For the digital filter, another limiting case of interest is when two transients with a 10-fold difference are closely spaced, i.e., when a vanishing peak follows a larger transient.[38] Figure 7a,b shows simulated signals with noise superimposed (see Figure S11 for details). These correspond to higher frequencies than our instrumentation can achieve but that are found in the literature for high-frequency studies with amplifiers with faster rise times (τ = 200 μs, $f_{c,inst}$ = 10 kHz, e.g., a Dagan Corp. Chem-Clamp amplifier). We apply a Butterworth low-pass filter to the simulated model transients. The cutoff frequency, f_c, is 156 Hz and $1/f_c$ = 6.4 ms, consistent with eq 10. For a digital filter, we expect a signal overshoot of the first transient and oscillations of around 10%, before the filter settles to a steady state. The 10% oscillations are comparable to the magnitude of the subsequent vanishing nanoimpact. However, we show here that digital filtering helps resolve small transients for both spikes and steps (Figure 7a,b, respectively). The blip response is simulated using a quadratic decay proposed for kinetically limited nanoimpacts[73] and that we observed for ZnO.[41]

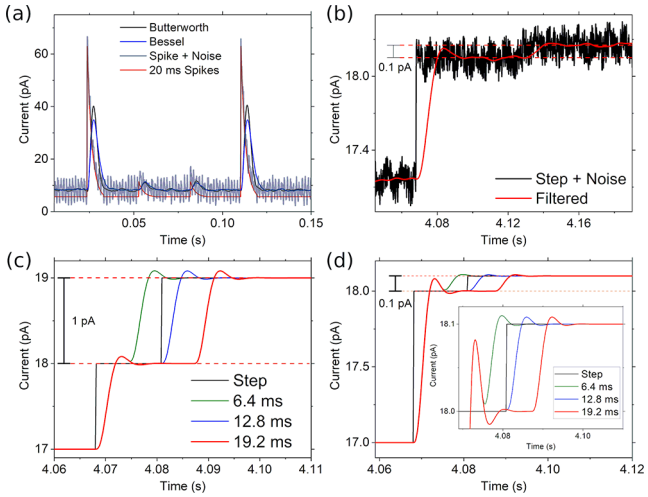

Figure 7. Digital filtering of simulated transients. (a) Spikes (red), after adding noise (gray) and after digital filtering (blue Bessel and black Butterworth, see text for details). (b) Simulated steps transients with noise (black) and after the filter (red). The inset in panel b shows the ringing that follows the first step. (c and d) Step function and the effect of a Butterworth digital filter on closely spaced events. Δt_{col} is the time lapsed after the first event. (c) First step 1 pA followed by a 1 pA event, (d) 1 pA step followed by 0.1 pA event; in both panels c and d the time after the first event is Δt_{col} = 6.4, 12.8, and 19.2 ms.

Closely Spaced Step Transients. Figure 7b−d shows the simulation of closely spaced steps. We present two cases: a 1 pA step followed by (1) a step of equal magnitude depicted in Figure 7c, and (2) a 0.1 pA step closely after the first 1-pA-step (Figure 7d). However, the step size is arbitrary, and this analysis applies to steps followed by an equal step or a second step with a tenth of the magnitude. Figure 7c shows that two consecutive steps of the same size can readily be resolved when the steps occur with a spacing of $\geq 1/f_c$. In contrast, the smaller subsequent steps cannot be resolved until time of $3(1/f_c)$ has elapsed from the larger step, Figure 7d. This is in agreement with literature values[39,64] and Figure 7b, where $k_{samp} \geq 3$. Further effects of the time constant and the shape of the following signals are discussed in the SI, section S13.

Figure S13 shows simulations of steps that are filtered with Bessel and Butterworth low pass filters. The step transients occur after the filters have reached their steady state, and the frequencies are within the sampling requirements given above by eq 12. Interestingly, the Bessel filter only reaches the final transient when the filtering cutoff is <0.3 f_s (or <0.6 f_{max}). If the filter cutoff is higher than 0.3 f_s, the steady state value of the step becomes 0.84 pA. This value is lower than the simulated 1 pA, exactly, and after 13 steps, the error is cumulative 13 × 0.16 pA = 2 pA. Therefore, there is an offset on the steady-state value which is 2 pA lower than the simulated final value (SI, section 12, Figure S13). However, the Bessel filter is more robust which allows us to filter at higher frequencies, without the error observed with the Bessel filter.

https://dx.doi.org/10.1021/acs.analchem.9b05238
Anal. Chem. 2020, 92, 8704−8714

Spike Signals. A similar analysis of spike transients is shown in Figure S14. The spikes have different times between consecutive collision times, Δt_{col}, 7, 20, and 50 ms. As a result of the filtering, the small vanishing peaks (see Figure 7a, gray curve) are evident after noise removal, regardless of the time elapsed between small and large spikes, see Figure S15. As discussed in the SI (section 13), digital filtering can complicate integrating closely spaced spikes. The effect of filtering is minimal when the signal does not include noise of around 10× the smaller peaks, where the errors are the largest of approximately −30%. (Tables S7 and S8). When the synthetic noise function does not include random noise the error is much smaller (Table S9), indicating that removing noise with uniform power across the frequency spectrum is responsible for this artifact. In summary, digital filtering is effective at detecting closely spaced spike transients. However, the area is not always preserved when a small peak (1/10th of the first one) closely follows the first transient, especially when the signal is smaller than the noise with a uniform spectral distribution. This observation indicates that the algorithm may be limited in removing thermal noise when the signal is ∼1/10th of the noise. However, this is an extreme case, and while the algorithm allows us to resolve the transients, the area is underestimated.

Overall, we found that eqs 9−11 set an acceptable sampling rate to resolve the transients with enough mechanistic information. Using digital filtering can remove a specific noise region of the spectrum in a data set with enough resolution for both steps and spikes. When using digital filtering protocols, one must verify that the charge is preserved when a region of the frequency spectra is removed. For steps, the time it takes the filter to reach steady state limits the frequency available to resolve closely spaced transients. For spikes, the resolution of the spike is less problematic, but the area may not be preserved when filtering thermal noise larger than the signal.

CONCLUSION

We demonstrated the use of digital frequency analysis in single entity electrochemical transient experiments to discriminate against noise. Moreover, this protocol could allow detecting stochastic processes related to nanoimpacts and provide information about the electrochemistry of single entities. This could lead to new insights into the processes occurring at the electrode−NP interface. For example, the background processes appear at distinct frequencies that do not always correlate with the photoelectrochemical detection of TiO_2 NPs transients. On the other hand, FFT combined with third-order Butterworth digital filters increases S/N while minimizing signal distortion. In three different types of experiments, single NP electrocatalytic amplification, photocatalytic amplification, and nanoimpacts of individual entities, digital filtering discriminates against noise with the Butterworth filters minimizing signal distortion. In contrast, the rectangle filter is an effective and straightforward alternative to filter noise and design a more complicated digital filter. In transient peak analysis, the area is preserved in the nanoimpact experiments when the signal is not convoluted with noise that is larger than the signal, and with a uniform spectral distribution across the sampled frequency spectrum. In hydrazine oxidation by single Au NPs, we determined the limits of digital filtering, where it does not affect the step height. This feature is critical for sizing applications, where the stepwise change of the particle-by-particle current is used to determine NP radius. In electrolysis experiments that model nanoimpacts, sampling data at rates higher than the fundamental collision frequency, f_p, caused the data acquisition to overlap with environmental noise. The use of a band-stop Butterworth filter removes noise in the intermediate region of the frequency domain experiment while preserving the fundamental shape of the current transient. One drawback of digital filtering is that it introduces a delay due to the frequency response of the filters. In this work, the delay is in the order of 70 ms for cutoff frequencies of 5 to 20 Hz (less than 35 ms for band-stop of 12.5 to 150 Hz), and we discuss an approximation for the high pass[61] and extend it to the band-stop Butterworth filters. However, note that this shift in phase (time) is also present in analog filters, widely used in electrochemical instrumentation. The digital filtering protocol can be used to design an analog filter custom-built for the application of interest. This approach takes advantage of the sampling rate currently available. After analysis of the FFT spectrum of the collisions and their blanks, we can determine the optimal frequency range a posteriori. Moreover, with a digital Butterworth low pass filter, it is possible to minimize the time delay by correcting the phase shift with a double-pass infinite impulse response algorithm (IIR) to yield a zero-phase filter,[35,66] and the implementation of this IIR algorithm will be the objective of future work. Our group is also investigating the background frequency spectrum to obtain reliable data in single NP photoelectrochemistry experiments that will be reported in due time.[74]

ASSOCIATED CONTENT

Supporting Information

The Supporting Information is available free of charge at https://pubs.acs.org/doi/10.1021/acs.analchem.9b05238.

Details of FFT theory, simulations, and experimental methods (PDF)

AUTHOR INFORMATION

Corresponding Author

Mario A. Alpuche-Aviles − *Department of Chemistry, University of Nevada, Reno, Nevada 89557, United States;* orcid.org/0000-0003-2615-4115; Email: malpuche@unr.edu

Authors

Salvador Gutierrez-Portocarrero − *Department of Chemistry, University of Nevada, Reno, Nevada 89557, United States*

Kiley Sauer − *Department of Chemistry, University of Nevada, Reno, Nevada 89557, United States*

Nelum Karunathilake − *Department of Chemistry, University of Nevada, Reno, Nevada 89557, United States*

Pradeep Subedi − *Department of Chemistry, University of Nevada, Reno, Nevada 89557, United States*

Complete contact information is available at: https://pubs.acs.org/10.1021/acs.analchem.9b05238

Notes

The authors declare no competing financial interest.

ACKNOWLEDGMENTS

The authors acknowledge funding through the National Science Foundation (NSF) Career Award for M.A.A., CHE 1255387, and NSF CHE 1905312. The electrodes were

characterized using an SEM funded with NSF Grant MRI 1726897. We thank Zachary Karmiol of UNR, who collected the TEM images, and Dr. Joaquín Flores for the fruitful discussion on FFT.

REFERENCES

(1) Park, J. H.; Thorgaard, S. N.; Zhang, B.; Bard, A. J. *J. Am. Chem. Soc.* **2013**, *135*, 5258−5261.
(2) Alpuche-Aviles, M. A.; Gutiérrez-Portocarrero, S.; Barakoti, K. K. *Curr. Opin. Electrochem.* **2019**, *13*, 174−180.
(3) Bard, A. J.; Zhou, H.; Kwon, S. J. *Isr. J. Chem.* **2010**, *50*, 267−276.
(4) Kwon, S. J.; Zhou, H.; Fan, F.-R. F.; Vorobyev, V.; Zhang, B.; Bard, A. J. *Phys. Chem. Chem. Phys.* **2011**, *13*, 5394−5402.
(5) Pumera, M. *ACS Nano* **2014**, *8*, 7555−7558.
(6) Rees, N. V. *Electrochem. Commun.* **2014**, *43*, 83−86.
(7) Sokolov, S. V.; Eloul, S.; Kätelhön, E.; Batchelor-McAuley, C.; Compton, R. G. *Phys. Chem. Chem. Phys.* **2017**, *19*, 28−43.
(8) Xiao, X.; Fan, F.-R. F.; Zhou, J.; Bard, A. J. *J. Am. Chem. Soc.* **2008**, *130*, 16669−16677.
(9) Fernando, A.; Parajuli, S.; Alpuche-Aviles, M. A. *J. Am. Chem. Soc.* **2013**, *135*, 10894−10897.
(10) Ma, H.; Ma, W.; Chen, J. F.; Liu, X. Y.; Peng, Y. Y.; Yang, Z. Y.; Tian, H.; Long, Y. T. *J. Am. Chem. Soc.* **2018**, *140*, 5272−5279.
(11) Bartlett, T. R.; Sokolov, S. V.; Compton, R. G. *Russ. J. Electrochem.* **2016**, *52*, 1131−1136.
(12) Sardesai, N. P.; Andreescu, D.; Andreescu, S. *J. Am. Chem. Soc.* **2013**, *135*, 16770−16773.
(13) Dasari, R.; Robinson, D. A.; Stevenson, K. J. *J. Am. Chem. Soc.* **2013**, *135*, 570.
(14) Zhou, H.; Fan, F.-R. F.; Bard, A. J. *J. Phys. Chem. Lett.* **2010**, *1*, 2671−2674.
(15) Zhou, Y. G.; Rees, N. V.; Compton, R. G. *Chem. Phys. Lett.* **2011**, *511*, 183−186.
(16) Zhou, Y. G.; Rees, N. V.; Compton, R. G. *ChemPhysChem* **2011**, *12*, 2085−2087.
(17) Zhou, Y.-G.; Rees, N. V.; Compton, R. G. *Angew. Chem., Int. Ed.* **2011**, *50*, 4219−4221.
(18) Kim, J.; Kim, B.-K.; Cho, S. K.; Bard, A. J. *J. Am. Chem. Soc.* **2014**, *136*, 8173−8176.
(19) Hill, C. M.; Kim, J.; Bard, A. J. *J. Am. Chem. Soc.* **2015**, *137*, 11321−11326.
(20) Anderson, T. J.; Zhang, B. *Acc. Chem. Res.* **2016**, *49*, 2625−2631.
(21) Li, Y.; Cox, J. T.; Zhang, B. *J. Am. Chem. Soc.* **2010**, *132*, 3047−3054.
(22) Sun, T.; Wang, D.; Mirkin, M. V. *Angew. Chem., Int. Ed.* **2018**, *57*, 7463−7467.
(23) Sun, T.; Yu, Y.; Zacher, B. J.; Mirkin, M. V. *Angew. Chem., Int. Ed.* **2014**, *53*, 14120−14123.
(24) Park, J. H.; Boika, A.; Park, H. S.; Lee, H. C.; Bard, A. J. *J. Phys. Chem. C* **2013**, *117*, 6651−6657.
(25) Betty, K. R.; Horlick, G. *Appl. Spectrosc.* **1976**, *30*, 23−27.
(26) Horlick, G. *Anal. Chem.* **1972**, *44*, 943−947.
(27) Ernst, R. R.; Anderson, W. A. *Rev. Sci. Instrum.* **1966**, *37*, 93−102.
(28) Rabenstein, D. L. *Anal. Chem.* **2001**, *73*, 214−223.
(29) Davis, S. P.; Abrams, M. C.; Brault, J. W. *Fourier transform spectrometry*; Academic Press: San Diego, 2001; p 262.
(30) De Levie, R.; Sarangapani, S.; Czekaj, P. *Anal. Chem.* **1978**, *50*, 110−115.
(31) Glover, D. E.; Smith, D. E. *Anal. Chem.* **1973**, *45*, 1869−1877.
(32) Smith, D. E. *Anal. Chem.* **1976**, *48*, 517A−526a.
(33) Smith, D. E. *Anal. Chem.* **1976**, *48*, 221A−240A.
(34) Wipf, D. O.; Kristensen, E. W.; Deakin, M. R.; Wightman, R. M. *Anal. Chem.* **1988**, *60*, 306−310.
(35) Atcherley, C. W.; Vreeland, R. F.; Monroe, E. B.; Sanchez-Gomez, E.; Heien, M. L. *Anal. Chem.* **2013**, *85*, 7654−7658.
(36) Keithley, R. B.; Takmakov, P.; Bucher, E. S.; Belle, A. M.; Owesson-White, C. A.; Park, J.; Wightman, R. M. *Anal. Chem.* **2011**, *83*, 3563−3571.
(37) Heien, M. L. A. V.; Phillips, P. E. M.; Stuber, G. D.; Seipel, A. T.; Wightman, R. M. *Analyst* **2003**, *128*, 1413−1419.
(38) Little, C. A.; Xie, R.; Batchelor-McAuley, C.; Kätelhön, E.; Li, X.; Young, N. P.; Compton, R. G. *Phys. Chem. Chem. Phys.* **2018**, *20*, 13537−13546.
(39) Kanokkanchana, K.; Saw, E. N.; Tschulik, K. *ChemElectroChem* **2018**, *5*, 3000−3005.
(40) Edwards, M. A.; Robinson, D. A.; Ren, H.; Cheyne, C. G.; Tan, C. S.; White, H. S. *Faraday Discuss.* **2018**, *210*, 9−28.
(41) Karunathilake, N.; Gutierrez-Portocarrero, S.; Subedi, P.; Alpuche-Aviles, M. A. *ChemElectroChem* **2020**, *7*, 2248−2257.
(42) Marks, R. J. I. *Introduction to Shannon sampling and interpolation theory*; Springer Science & Business Media: Berlin, 2012.
(43) Marvasti, F. *Nonuniform sampling: theory and practice*; Springer Science & Business Media: Berlin, 2012.
(44) Oppenheim, A. V.; Wilsky, A. S. *Signals and systems*; Pearson: London, 2013.
(45) Orfanidis, S. J. *Introduction to signal processing*; Prentice Hall: Upper Saddle River, NJ, 1996.
(46) Hieftje, G.; Holder, B.; Maddux, A.; Lim, R. *Anal. Chem.* **1973**, *45*, 277−284.
(47) Wightman, R. M.; Wipf, D. O. In *Electroanal. Chem.* Bard, A. J., Ed.: 1989; pp 267−353.
(48) Mauzeroll, J.; LeSuer, R. J. In *Handbook of electrochemistry*; Zoski, C. G., Ed.; Elsevier: New York, 2007; pp 199−211.
(49) Kim, D. Y.; Lee, S.; Kwon, S. J. *Bull. Korean Chem. Soc.* **2015**, *36*, 678−681.
(50) Barakoti, K. K.; Parajuli, S.; Chhetri, P.; Rana, G. R.; Kazemi, R.; Malkiewich, R.; Alpuche-Aviles, M. A. *Faraday Discuss.* **2016**, *193*, 313−325.
(51) Fernando, A.; Chhetri, P.; Barakoti, K. K.; Parajuli, S.; Kazemi, R.; Alpuche-Aviles, M. A. *J. Electrochem. Soc.* **2016**, *163*, H3025−H3031.
(52) Alpuche-Aviles, M. A.; Wu, Y. *J. Am. Chem. Soc.* **2009**, *131*, 3216−3224.
(53) Perera, N.; Karunathilake, N.; Chhetri, P.; Alpuche-Aviles, M. A. *Anal. Chem.* **2015**, *87*, 777−784.
(54) Wehmeyer, K. R.; Wightman, R. M. *Anal. Chem.* **1985**, *57*, 1989−1993.
(55) Kätelhön, E.; Feng, A.; Cheng, W.; Eloul, S.; Batchelor-McAuley, C.; Compton, R. G. *J. Phys. Chem. C* **2016**, *120*, 17029−17034.
(56) Bobbert, P. A.; Wind, M. M.; Vlieger, J. *Phys. A* **1987**, *141*, 58−72.
(57) Karp, S.; Meites, L. *J. Am. Chem. Soc.* **1962**, *84*, 906−912.
(58) Horowitz, P.; Hill, W. In *The art of electronics*; Cambridge University Press: New York, 1989; pp 270−274.
(59) Cunningham, E. P. *Digital Filtering: An Introduction*; Wiley: Weinheim, Germany, 1996.
(60) Boika, A.; Bard, A. J. *Anal. Chem.* **2015**, *87*, 4341−4346.
(61) Manal, K.; Rose, W. *J. Biomech.* **2007**, *40*, 678−681.
(62) Kang, M.; Perry, D.; Kim, Y.-R.; Colburn, A. W.; Lazenby, R. A.; Unwin, P. R. *J. Am. Chem. Soc.* **2015**, *137*, 10902−10905.
(63) Oja, S. M.; Robinson, D. A.; Vitti, N. J.; Edwards, M. A.; Liu, Y.; White, H. S.; Zhang, B. *J. Am. Chem. Soc.* **2017**, *139*, 708−718.
(64) Robinson, D. A.; Liu, Y.; Edwards, M. A.; Vitti, N. J.; Oja, S. M.; Zhang, B.; White, H. S. *J. Am. Chem. Soc.* **2017**, *139*, 16923−16931.
(65) Ustarroz, J.; Kang, M.; Bullions, E.; Unwin, P. R. *Chemical Science* **2017**, *8*, 1841−1853.
(66) Kormylo, J.; Jain, V. *IEEE Trans. Acoust., Speech, Signal Process.* **1974**, *22*, 384−387.
(67) Chen, C.-H.; Ravenhill, E. R.; Momotenko, D.; Kim, Y.-R.; Lai, S. C. S.; Unwin, P. R. *Langmuir* **2015**, *31*, 11932−11942.
(68) Robinson, D. A.; Edwards, M. A.; Ren, H.; White, H. S. *ChemElectroChem* **2018**, *5*, 3059−3067.

https://dx.doi.org/10.1021/acs.analchem.9b05238
Anal. Chem. 2020, 92, 8704−8714

(69) Ma, W.; Ma, H.; Chen, J.-F.; Peng, Y.-Y.; Yang, Z.-Y.; Wang, H.-F.; Ying, Y.-L.; Tian, H.; Long, Y.-T. *Chemical Science* **2017**, *8*, 1854−1861.
(70) Binkley, D.; Dessy, R. *J. Chem. Educ.* **1979**, *56*, 148.
(71) Batchelor-McAuley, C.; Ellison, J.; Tschulik, K.; Hurst, P. L.; Boldt, R.; Compton, R. G. *Analyst* **2015**, *140*, 5048−5054.
(72) Kätelhön, E.; Tanner, E. E. L.; Batchelor-McAuley, C.; Compton, R. G. *Electrochim. Acta* **2016**, *199*, 297−304.
(73) Singh, P. S.; Kätelhön, E.; Mathwig, K.; Wolfrum, B.; Lemay, S. G. *ACS Nano* **2012**, *6*, 9662−9671.
(74) Gutierrez-Portocarrero, S.; Chhetri, P.; Subedi, P.; Victors, A.; Alpuche-Aviles, M. A. *in preparation* **2020**.

https://dx.doi.org/10.1021/acs.analchem.9b05238
Anal. Chem. 2020, 92, 8704−8714